*J. Fluid Mech.* (1972), *vol.* 54, *part* 3, *pp.* 427–448
*Printed in Great Britain*



# Microscale pressure fluctuations near waves being generated by the wind

By J. A. ELLIOTT†
Institute of Oceanography, University of British Columbia, Vancouver

(Received 18 June 1971 and in revised form 15 April 1972)

Measurements of static pressure and wave height are used to describe the wave-induced pressure field above generating sea waves. A large hump in the pressure spectra is observed at the wave frequencies. The amplitude of this hump increases and the rate of its vertical decay decreases as the mean wind speed increases. The phase difference between the pressure and the waves during active generation is about 135°, pressure lagging the waves, and does not change vertically for measurements at heights greater than the wave crests. In the present data, active wave generation appears to occur only when the wind at a height of 5 metres is greater than or about equal to twice the phase speed of the waves.

## 1. Introduction

When sea waves are being generated by the wind there is, adjacent to the water surface, an air layer in which energy is being transferred to a pressure field which is generating the waves. The study of wave generation is the study of this region near the water surface. Most experimental data on the wave-generation problem have come from wind–water tunnels. Shemdin & Hsu (1967) measured the static pressure near a propagating wave in a wind–water tunnel and were able to evaluate mean phase angles between the pressure and wave height. They considered their results to be in agreement with the theoretical predictions of the Miles–Benjamin theory. Unfortunately, it is difficult to simulate in the laboratory 'typical' air turbulence or 'typical' sea states; ideally, observations in a natural environment are required. A recent example of observations taken under natural conditions is the work of Dobson (1971), who has measured the energy flux to surface waves directly by measuring the static pressure on the water surface with a floating instrument. His measurements indicate that a large fraction of the momentum transferred to the water is through the waves. Dobson's measured mean phase angles between the pressure and the waves were significantly larger than those obtained by Shemdin & Hsu.

In the present study, Eulerian measurements of the fluctuations in static pressure and in the downstream velocity were taken at a short distance above the crests of sea waves. Power spectra and cross-spectra are used to describe the relationships between the pressure, downstream velocity and the waves.

† Present address: Bedford Institute, Dartmouth, N.S., Canada.

## 2. Experimental and analytic technique

### 2.1. *Site*

The observations were made at a fetch-limited site on the south side of English Bay at Vancouver, British Columbia. This site has been used previously by the Institute of Oceanography, University of British Columbia and is described in Pond, Smith, Hamblin & Burling (1966). It is also the site used by Dobson (1971). The site is located on a tidal flat; observations were taken when the water was 3–4 m deep. There are two common wind directions, easterly with a fetch of about 7 km and westerly with a fetch of about 50 km. The statistics of the wave field for east winds have been thoroughly studied by Garrett (1969). His measurements indicate that the non-uniform fetch, which produces some asymmetry in the directional spectra, does not prevent the power spectrum of the waves from attaining the equilibrium form; that is, the power spectrum has an approximate fall-off of $n^{-5}$, where $n$ is frequency (Phillips 1966, p. 109 ff.).

### 2.2. *Instrumentation*

Sensors were mounted on a mast located about 50 m from a recording platform. A $1\frac{1}{2}$ m long capacitance wave probe (Hume 1969) was positioned such that it operated near its midpoint; velocity and one or two pressure sensors were fixed at heights of about 30–100 cm above the midpoint of the wave probe. The static pressure measurements were obtained using instrumentation described by Elliott (1970). A Disa constant-temperature anemometer (U-wire) was used for measuring downstream velocity fluctuations. All these instruments give the amplitude to $\pm 10\,\%$ or better and the phase to within a few degrees. The positions at which the wave height, pressure and velocity were measured were as nearly as was practical in a line perpendicular to the mean wind direction, that is, along the wave crests. The spacing cross wind between sensors was typically 5–10 cm. Underwater cables transferred the signals from these sensors to the nearby platform, where the information was recorded on magnetic tape as FM signals.

The mean wind speed was obtained from a cup anemometer profile system consisting of four cups, logarithmically spaced at between 0·5 and 2 m. The wind speed at levels different from the cup positions was read graphically from a plot of the measured profile. Wind speeds were adjusted to give values relative to the mean current.

Other data recorded periodically during each set of observations included the wind direction, mean current, wet and dry bulb temperatures and water temperature.

### 2.3. *Analysis*

The analog data were analysed digitally. To prevent significant aliasing, the signals were first passed through low-pass linear phase shift filters. Then, after digitizing, a 'fast Fourier transform' algorithm was employed to produce the complex Fourier coefficients of the data and from these the power spectrum

$\Phi(n)$, coherence and phase. The definition used for the coherence between signals 1 and 2 is

$$\{[S_{12}^2(n)+Q_{12}^2(n)]/\Phi_1(n)\,\Phi_2(n)\}^{\frac{1}{2}}, \tag{1}$$

where $S$ and $Q$ are the cospectrum and the quadrature spectrum respectively. Other definitions are equivalent to those given by Blackman & Tukey (1959, pp. 167–178).

Some of the low frequency waves measured at the site were affected by the water depth $h$. This influence was taken into account whenever calculations were required to evaluate the wavelength $k$ or phase speed $C$ for a given wave frequency. Under these circumstances the values of $k$ and $C$ were obtained from the solution for small amplitude gravitational waves: $C^2 = gk^{-1}\tanh kh$ and $n = kC(2\pi)^{-1}$. In most cases the result was within 10% of the assumption of infinite depth. For example, waves of period 3 s were typically the longest waves observed. These waves have a wavenumber $k = 2\pi/\lambda_w$ of about $4{\cdot}9 \times 10^{-3}\,\mathrm{cm}^{-1}$ in 3 m of water as compared with $4{\cdot}5 \times 10^{-3}\,\mathrm{cm}^{-1}$ in water of infinite depth.

The stability of the air over the water was estimated for each of the observation periods in terms of the gradient Richardson number $Ri_G$. This was evaluated in a difference form employing geometric means. A virtual temperature was used in order to include the effect of both air temperature and humidity on the buoyancy. This method of estimating the stability should give at least an order-of-magnitude value.

## 3. Results

Fourteen data runs of about 15 min duration were obtained under a variety of wind–wave conditions. For convenience of comparison, information relating to the different runs is set out in table 1. The runs are broken into four groups labelled $A$, $B$, $C$ and $D$ on the basis of the wind speed relative to the phase speed of the fastest waves. Within each group wind–wave conditions were similar and therefore the results from each group are similar.

Sample wave spectra representative of each of the four groups are shown in figure 1. These spectra exhibit properties that are considered typical of a fully developed wave field: at high frequencies there is a power-law behaviour (the spectra have a slope of $-4{\cdot}5$ to $-5$), which is terminated at the peak of the spectrum by a nearly vertical drop-off. The lowest frequency that has the equilibrium form (with a slope of approximately $-5$) is referred to as the 'equilibrium peak'. Some of the wave spectra, particularly that for run 119/2 (figure 1), have relatively large amounts of energy at frequencies lower than the equilibrium peak. This energy is thought to be a result of the non-uniform fetch; the waves associated with this energy are not part of the locally generated wave field but are propagating into the area.

The velocity difference $(U_5 - C)_p$ between the measured wind at a height of 5 m ($U_5$) and the calculated phase speed of the waves at the frequency of the equilibrium peak is given in the last column of table 1. The number given in brackets after this velocity difference is the wave frequency at the equilibrium peak. As was mentioned above, $(U_5 - C)_p$ is the basis for grouping the observations,

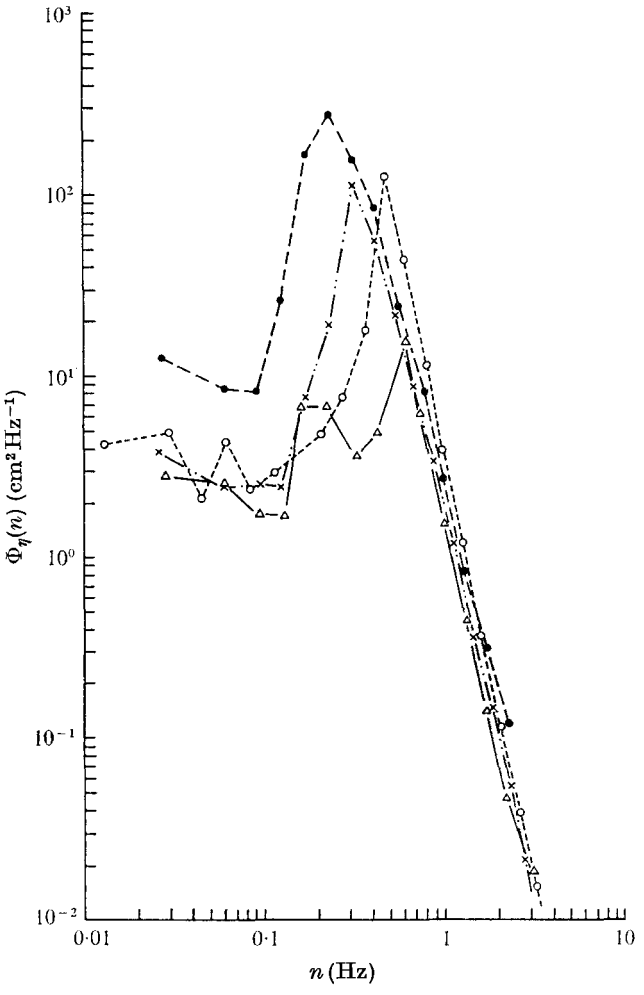


FIGURE 1. Typical wave spectra. ○, run 167/2, group $A$; △, run 119/2, group $B$; ×, run 80/3, group $C$; ●, run 164/1, group $D$.

and most of the data will be discussed in terms of these groups rather than as individual runs. This grouping is in most cases a natural one in that, except for one case, the runs within each group were taken sequentially on a given day when wind–wave conditions remained relatively constant (see table 1).

In group $A$ the winds were from the east at about 7·5 m s$^{-1}$. The measured root-mean-square wave amplitude was about 6 cm and the wave spectra of the sequence are almost identical, implying steady-state fetch-limited conditions during the observations. The wind at a height of 5 m was about 4·5 m s$^{-1}$ faster than the phase speed of the waves at the frequency of the equilibrium peak. The data from group $B$ showed a slowly growing wave field under relatively steady east winds which averaged about 4·5 m s$^{-1}$. For this group $(U_5 - C)_p$ was about 2 m s$^{-1}$. The data in group $C$ were recorded during west winds. The wave spectra for all the runs are similar, with a root-mean-square amplitude of about 6 cm.

| Run | Date | Time (PST) | Static pressure | Velocity | Duration (min) | $U_5$ (m s$^{-1}$) | Wind direction | $Ri_G$ | $\tau$ (dyn cm$^{-2}$) | $z$ (m) | $U$ (m s$^{-1}$) | $h$ (m) | $U_w$ (m s$^{-1}$) | $(U_5-C)_p$ (m s$^{-1}$) |
|---|---|---|---|---|---|---|---|---|---|---|---|---|---|---|
| | Group *A* | | | | | | | | | | | | | |
| 167/1/1 | 14 December 1968 | 1209–1228 | X | — | 19 | 8·1 | 115 | 0·02 | 0·985 | 0·50 | 6·3 | 3·5 | 0·24E | 5·0 (0·50) |
| 167/1/2 | 14 December 1968 | 1228–1246 | X | — | 18 | 7·2 | 120 | 0·02 | 0·776 | 0·50 | 5·7 | 3·5 | 0·24E | 4·1 (0·50) |
| 167/2 | 14 December 1968 | 1252–1306 | X | — | 14 | 7·9 | 100 | 0·03 | 0·935 | 0·30 | 5·8 | 3·5 | 0·24E | 4·8 (0·50) |
| 167/3 | 14 December 1968 | 1312–1318 | X | — | 6 | 6·4 | 125 | 0·05 | 0·615 | 0·30 | 4·8 | 3·5 | 0·24E | 3·3 (0·50) |
| | Group *B* | | | | | | | | | | | | | |
| 60/4 | 2 April 1969 | 1650–1712 | X | X | 22 | 4·1 | 130 | −0·05 | 0·252 | 0·30 | 2·9 | 3·0 | 0 | 1·7 (0·65) |
| | | | X | | | | | | | 0·80 | 3·3 | | | |
| 119/1 | 2 April 1969 | 1745–1800 | X | X | 15 | 4·1 | 90 | −0·05 | 0·252 | 0·40 | 3·5 | 3·0 | 0 | 1·8 (0·70) |
| | | | X | | | | | | | 0·90 | 3·7 | | | |
| 119/2 | 2 April 1969 | 1820–1840 | X | X | 19 | 4·7 | 120 | −0·04 | 0·331 | 0·30 | 4·1 | 3·0 | 0 | 2·3 (0·65) |
| | | | X | | | | | | | 0·80 | 4·3 | | | |
| 119/3 | 2 April 1969 | 1850–1908 | X | — | 17 | 4·8 | 120 | −0·04 | 0·344 | 0·30 | 3·8 | 3·0 | 0 | 2·2 (0·60) |
| | | | X | | | | | | | 0·80 | 4·2 | | | |
| | Group *C* | | | | | | | | | | | | | |
| 173/3 | 20 March 1969 | | X | X | 14 | 3·6 | 240 | 0·02 | 0·194 | 0·90 | 3·1 | 2·5 | 0·30W | −0·5 (0·30) |
| | | | X | | | | | | | 1·40 | 3·2 | | | |
| 60/1 | 27 March 1969 | 1140–1156 | X | X | 16 | 4·3 | 250 | −0·01 | 0·274 | 0·40 | 3·5 | 2·5 | 0·22E | 0·2 (0·32) |
| 60/2 | 27 March 1969 | 1214–1226 | X | X | 12 | 4·7 | 250 | 0·001 | 0·331 | 0·50 | 3·9 | 2·5 | 0·22E | 0·6 (0·32) |
| 80/3 | 27 March 1969 | 1112–1129 | X | X | 17 | 3·9 | 260 | −0·01 | 0·228 | 0·30 | 3·3 | 2·5 | 0·22E | −0·2 (0·32) |
| | Group *D* | | | | | | | | | | | | | |
| 164/1 | 18 December 1968 | 1408–1422 | X | X | 14 | 2·6 | 290 | −0·19 | 0·101 | 0·50 | 2·2 | 3·5 | 0 | −2·3 (0·25) |
| 164/2 | 18 December 1968 | 1612–1625 | X | X | 16 | 4·1 | 340 | −0·09 | 0·252 | 0·60 | 3·5 | 3·5 | 0 | −1·5 (0·18) |

TABLE 1. Mean data for all runs. $U_5$ is the mean wind at 5 m, $Ri_G$ the gradient Richardson number, $\tau$ the surface stress (evaluated from a drag coefficient $C_D = 1{\cdot}2 \times 10^{-3}$ at 5 m and $U_5$), $z$ the instrument height, $U$ the mean wind at the instrument height, $h$ the water depth, $U_w$ the current and $(U_5-C)_p$ the value of $U_5-C$ at the equilibrium peak of the wave spectrum. X indicates that the variable was measured.

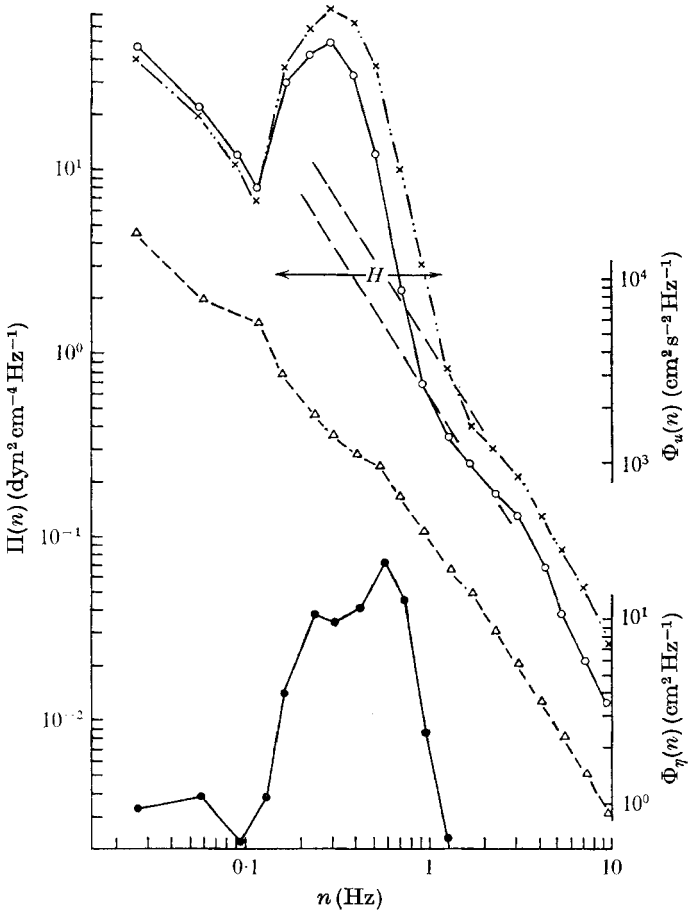


FIGURE 2. Pressure spectra $\Pi(n)$, downstream velocity spectra $\Phi_u(n)$ and wave spectra $\Phi_\eta(n)$ for run 119/2. ·· — × — ··, $p_u$; —○—, $p_L$; -- △ --, $u$; —●—, $\eta$.

For these waves $(U_5 - C)_p$ was nearly zero. Group $D$ data were recorded under light north-west winds and had a $(U_5 - C)_p$ of about $-2\,\mathrm{m\,s^{-1}}$. This situation in which the wave phase speed was faster than the wind speed at 5 m arose when there was a strong local wind ('Squamish') in an inlet near the site. Waves generated by this wind fanned out at the mouth of the inlet, some travelling into the English Bay region, which included the observation site.

The stability of the air column during all the runs (see table 1), estimated using the gradient Richardson number, was found to be nearly neutral and therefore not likely to be an important variable in the measurements.

### 3.1. *Static pressure*

3.1.1. *Amplitude.* A plot illustrating the typical characteristics of the spectra of static pressure fluctuations measured near the waves is given in figure 2. The data (run 119/2, group $B$) were collected from two pressure sensors with a vertical separation. The lower pressure sensor, measuring a pressure labelled $p_L$, was 30 cm

above the mean water level and the upper, measuring $p_U$ was at 80 cm. As shown in figure 2, the pressure spectra contain a 'hump' at the wave frequencies which is superimposed upon an otherwise monotonically sloped spectrum of the type that is normally found over a flat boundary (Elliott 1972). This hump is considered to be a wave-influenced pressure. The intensity in this humped part of the spectrum is up to ten times larger than the spectral intensity expected for a flat boundary under similar wind conditions. The extent in bandwidth of the hump is denoted, for convenience, by a double arrow labelled $H$. This hump is very similar to the wave spectrum but is not in exact proportion. For example, the slope on the high frequency side of the hump is not always $-4{\cdot}5$ to $-5$ as it is for the waves. The humped portion of the spectrum $p_U$ for the higher level pressure sensor is similar to that for the lower sensor $p_L$ but is smaller in amplitude, particularly at high frequencies, as would be expected. Remnants of the hump are observed during normal wave conditions up to heights $z$ between $\frac{1}{2}\lambda_w$ and $\lambda_w$, where $\lambda_w$ is the wavelength of the waves. This height $z$ can be estimated from the plots of the pressure spectra by using the highest frequency at which the hump is definable. For example, for run 173/3 this occurs for $p_U$ at a frequency $n \simeq 0{\cdot}9$ Hz. Waves of this frequency have a calculated wavelength $\lambda_w \simeq 200$ cm; the measurement height was 140 cm. For run 167/1/1 the corresponding figures are $n = 1{\cdot}5$ Hz, $\lambda_w = 70$ cm and $z = 30$ cm.

At higher frequencies than those of the 'humped' portion, the two pressure spectra $p_U$ and $p_L$ do not become superimposed as they do at the frequencies below the hump, $p_L$ being of higher intensity. Observations at similar levels over land and at higher elevations over water do not show this high frequency difference (Elliott 1972). However, the spectral slopes at higher frequencies than those of the hump are the same as those observed at similar heights over a flat boundary.

To compare the wave-influenced pressure $p_w$ observed in different runs and at different frequencies and heights, some measure of this pressure is required. The question arises as to what fraction of the pressure amplitude in the hump is associated directly with waves and what is associated with random turbulence. Since, as will be shown later, the coherence between the pressure and the waves at higher frequencies than those of the hump is essentially zero, that region of the spectrum can be said to result from random turbulence. It is assumed that the power law associated with the random turbulence in the frequency range of the hump will be similar to that observed outside it. Thus, as a first approximation the pressure amplitude $p_w$ in the hump associated directly with the waves may be taken to be the difference between the intensity measured and the straight-line projection from the high frequency tail (see dashed lines in figure 2). The values of $p_w$ would not differ by more than a few per cent, except at the highest frequencies of the hump, if the total pressure intensity were used instead. This pressure is not the same as the wave-induced pressure referred to by Phillips (1966, p. 80) in that $p_w$ is not entirely coherent with the waves (as will be shown below in §3.1.2).

A humped spectrum, similar to that observed at the wave frequencies, would be expected even if no mean wind or turbulence were present and a wave field were simply propagating past the pressure sensor. This case could be described

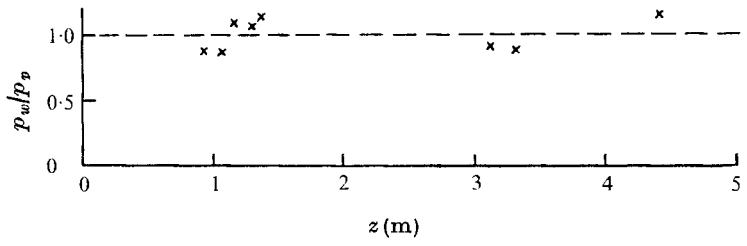


FIGURE 3. Ratio of measured to predicted pressure amplitude for propagating waves with no wind.

by a potential-flow solution (Lamb 1932, § 231). The pressure phase and magnitude ($p_p$) predicted by the potential-flow solution were checked in the field. Figure 3 shows the results obtained on days with a very light wind (a few cm/s) when a swell was propagating past the instrument mast. The pressure and wave height ($\eta_a$) were recorded on a strip-chart recorder instead of by the usual method of recording on magnetic tape. The values plotted each came from the average of about 100 estimates of individual amplitudes. The measured and predicted values agree to within about 10 %. As expected, phase differences between $p$ and $\eta$ were 180°, within the accuracy of the method. Thus potential-flow theory appears adequately to predict the pressure field (and hence supposedly the velocity field) for propagating waves in the absence of wind.

When there is a wind, potential-flow theory will not be expected to predict the pressure. The non-dimensional variables which might cause variations in the pressure $p_w$ associated with the waves are: $kz$, representative of the fractional height of the observations in terms of wavelength; $k\eta_a$, representative of the wave slope; and $U_5/C$, the ratio of the mean wind at 5 m to the phase speed of the waves. $\eta_a$, wave amplitude, can be approximated by $(2\Phi_\eta(n)\,\Delta n)^{\frac{1}{2}}$, where $\Phi_\eta(n)$ is the wave spectral density and $\Delta n$ is the one-half octave bandwidth for a narrow band of frequencies. When the wave spectrum has the equilibrium form the product $k\eta_a \simeq k(2\Phi_\eta(n)\,\Delta n)^{\frac{1}{2}}$ can be taken as a constant (Phillips 1966, p. 118). Pressure data from one 'fixed height' above mean water level and only for the frequency range where the waves have the equilibrium form are considered initially. In practice this 'fixed height' ranged from 30 to 50 cm. However, for this part of the data, $kz$ and $k\eta_a$ are approximately constant at any fixed frequency. In figure 4

$$p_w(n) = (2\Pi(n)\,\Delta n)^{\frac{1}{2}} - (2\Pi_0(n)\,\Delta n)^{\frac{1}{2}} \tag{2}$$

is plotted against $U_5/C$ with frequency as a parameter. $\Pi_0(n)$ is the background pressure spectrum illustrated by the dashed lines in figure 2. The points on the ordinate in figure 4 are derived from the limiting case of $U_5/C = 0$ and are assumed to be given at each frequency by the potential-flow solution

$$p_w(n) = \rho k(2\Phi_\eta(n)\,\Delta n)^{\frac{1}{2}}\,C^2\,e^{-kz}. \tag{3}$$

These potential-flow calculations use the mean values from the measured wave spectra and have $z = 40$ cm. As can be seen (figure 4), the data tend to group along lines which could be approximately extrapolated to the potential-flow

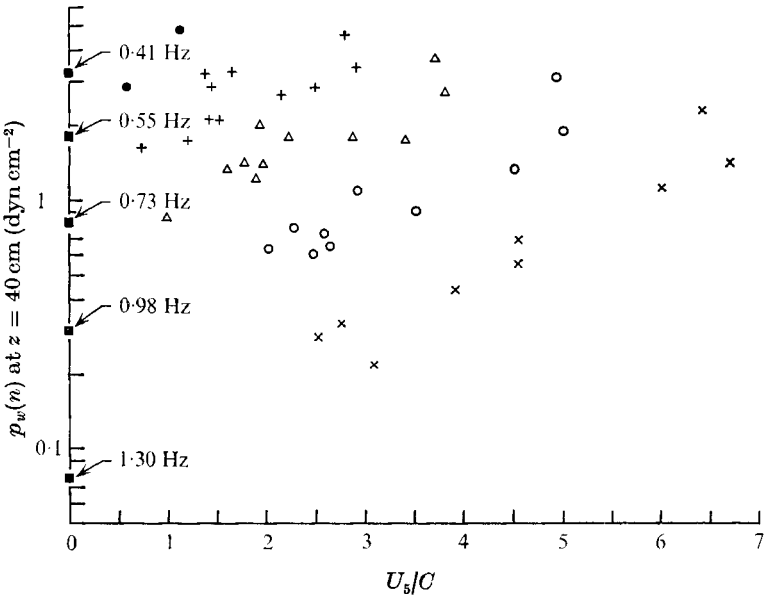


FIGURE 4. $p_w(n)$ at $z = 40$ cm at various constant frequencies for different values of $U_5/C$. The values plotted at $U_5/C = 0$ are for the potential-flow solution. ■, potential flow; ●, $n = 0{\cdot}41$ Hz; +, $n = 0{\cdot}55$ Hz; △, $n = 0{\cdot}73$ Hz; ○, $n = 0{\cdot}98$ Hz; ×, $n = 1{\cdot}30$ Hz.

calculations. As $U_5/C$ increases, the pressure intensity at all frequencies also increases. There is no indication of a distinctly different behaviour near $U_5 = C$.

With this plot (figure 4) as a background, data from all heights were considered in terms of the non-dimensional variables $kz$, $U_5/C$ and $p_w/p_0$, where

$$p_0 = \rho k(2\Phi_\eta(n)\,\Delta n)^{\frac{1}{2}}\,C^2. \tag{4}$$

The product $k(2\Phi_\eta(n)\,\Delta n)^{\frac{1}{2}}$ was chosen to be constant although it is not exactly so for this data, varying by about 20 %. This is not important provided that the role of $k\eta_a$ in $p_w$ is the same as in $p_0$. Two plots are used, figures 5(*a*) and (*b*), in which $p_w/p_0$ is shown as a function of $U_5/C$ at constant $kz$ and vice versa. The results in figure 5(*a*) are similar to those already shown in figure 4, with little change resulting from the additional data available for heights other than 30–50 cm. Straight lines representing constant values of $kz$ and $U_5/C$ have been drawn by hand among the data plotted in figures 5(*a*) and (*b*) respectively. It is felt that there is insufficient data to warrant a closer fitting of 'curves', and there are no theoretical predictions to act as guidelines. Acting as a first approximation, the data in figure 5, as represented by the lines shown, are summarized by the formula

$$p_w(n) = \rho k(2\Phi_\eta(n)\,\Delta n)^{\frac{1}{2}}\,C^2 \exp\left[0{\cdot}27U_5/C - kz(1 - 0{\cdot}08U_5/C)\right]. \tag{5}$$

The limiting case $U_5/C = 0$ is the potential-flow solution as given by (3). There is sufficient accuracy to show that, as $U_5/C$ increases, the slope of the lines in figure 5(*b*) decreases. Thus, as the wind increases, the vertical pressure decay at a given wavenumber is increasingly less than the exponential decay in potential flow.

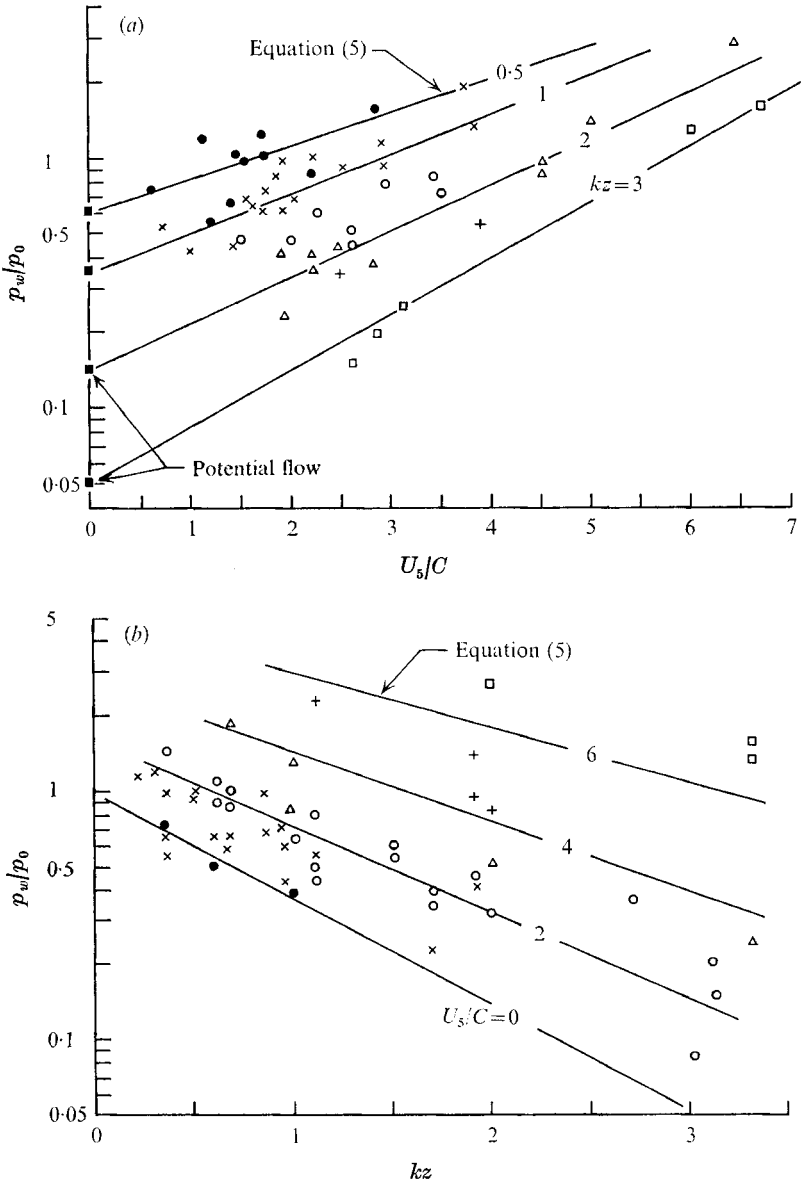


FIGURE 5. (*a*) $p_w/p_0$ for different values of $U_5/C$ at constant $kz$. ●, $kz$ = 0–0·5; ×, $kz$ = 0·5–1·0; ○, $kz$ = 1·0–1·5; △, $kz$ = 1·5–2·0; +, $kz$ = 2·0–2·5; ▲, $kz$ = 2·5–3·0; □, $kz$ = 3·0–3·5. (*b*) $p_w/p_0$ for different values of $kz$ at constant $U_5/C$. ●, $U_5/C$ = 0–1; ×, $U_5/C$ = 1–2; ○, $U_5/C$ = 2–3; △, $U_5/C$ = 3–4; +, $U_5/C$ = 4–5; ▲, $U_5/C$ = 5–6; □, $U_5/C$ = 6–7.

Equation (5), used to relate the observations to an empirical formulation, becomes physically unrealistic if extended to large values of $U_5/C$, beyond the data plotted. If $U_5/C = 12{\cdot}5$ is substituted into (5) all $z$ dependence disappears and at $U_5/C > 12{\cdot}5$ equation (5) has the pressure $p_w$ increasing vertically, the opposite of what would be expected to occur. This value of 12·5 for $U_5/C$ could

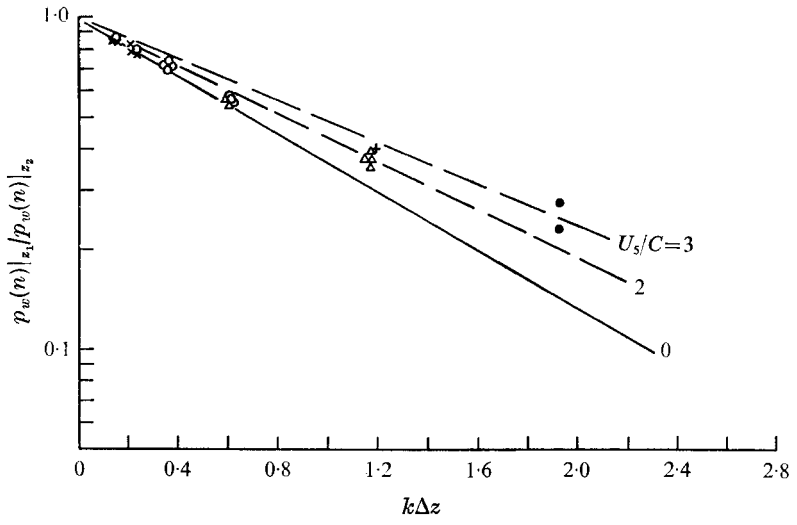


FIGURE 6. Ratio of the $p_w$ measured at two levels $z_1$ and $z_2$. The lines drawn are the predicted ratio from (6). ×, $U_5/C = 0{\cdot}5$–$1{\cdot}0$; ○, $U_5/C = 1{\cdot}1$–$1{\cdot}5$; △, $U_5/C = 1{\cdot}6$–$2{\cdot}0$; +, $U_5/C = 2{\cdot}1$–$2{\cdot}5$; ●, $U_5/C = 2{\cdot}6$–$3{\cdot}0$.

represent a wavelength of 10 cm and a $U_5$ of 5 m s$^{-1}$. Obviously, the formula given should not be extrapolated to regions outside that covered by the data, approximately $0 < U_5/C < 7$ and $0{\cdot}5 < kz < 3$, without caution, particularly at larger values of $U_5/C$.

It is possible to check the vertical dependence shown in (5) using simultaneous measurements at two levels (group *B*). By taking the ratio of the pressures $p_w(n)$ at the two levels, a $\Delta z$ dependence would be left. Using (5)

$$p_w(n)|_{z_1}/p_w(n)|_{z_2} = \exp\left[-k\Delta z + 0{\cdot}08(U_5/C)\,k\Delta z\right] \tag{6}$$

for $z_1 > z_2$. Measured values of this ratio and those calculated from (6) are compared in figure 6 for different $k\Delta z$. The fit is reasonable. Although not analysed in detail, individual calculations of the pressure intensity at frequencies lower than the frequency of the equilibrium peak gave results similar to those shown.

In summary, the wave-influenced pressure $p_w(n)$ has a magnitude which is similar to the potential-flow solution in very low winds; it increases monotonically as $U$ increases and decays vertically at a rate less than exponential; the higher the mean wind, the slower the decay.

The surface pressure spectra obtained by Dobson (1971) have a similar type of pressure hump, but in general they are not as well defined as those obtained in the present study (his low frequency intensities were in general an order of magnitude larger). There is some question as to how to compare Dobson's data with the present results since his instrument followed the water surface and hence his measurements were not Eulerian. Nevertheless, a comparison of Dobson's spectra (with and without $\rho g \eta_a$ removed) with values predicted by (5) with $z = 0$ agree reasonably well, within a factor of about 2. Therefore (5) may approximately predict the hump pressure $p_w(n)$ down to the wave surface.

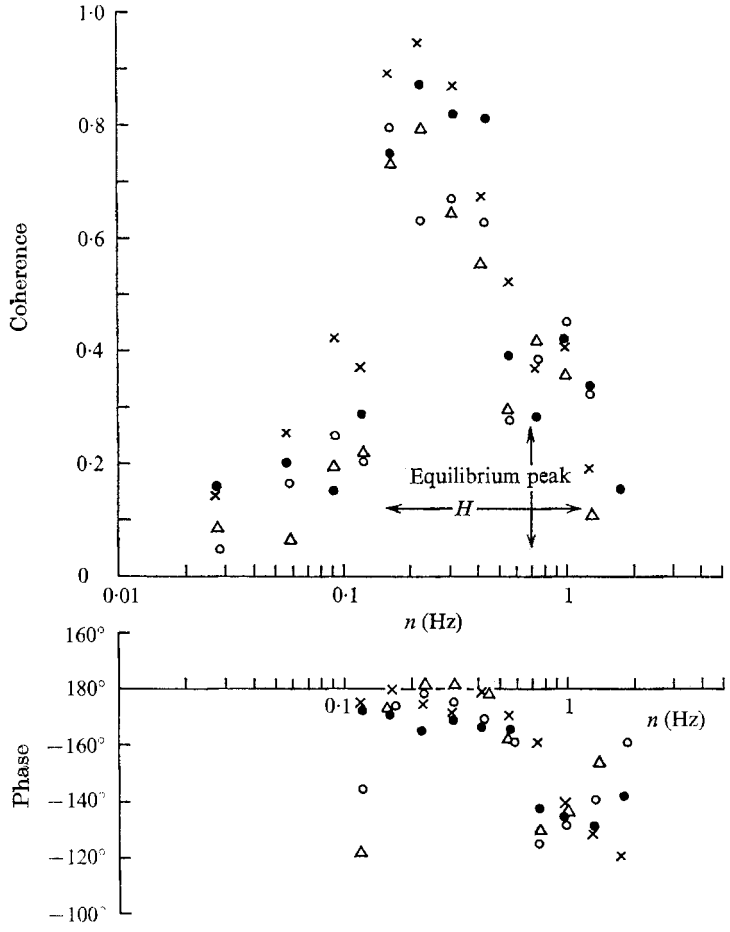


FIGURE 7. Coherence and phase between the pressure $p_L$ at the lower sensor and the waves $\eta$ for data group $B$. Phase positive means $p_L$ leads $\eta$. ●, run 60/4; ×, run 119/1; ○, run 119/2; △, run 119/3.

3.1.2. *Coherence and phase.* Since the data of group $B$ are the most detailed and are representative of information observed in the other groups, they will be used to illustrate the coherence and phase relationships found between the pressure and the waves. The coherence and phase between the lower pressure $p_L$ and the wave amplitude $\eta_a$ for the data in group $B$ are given in figure 7. Realizing that the pressure which generates the waves is the component of the pressure which is in quadrature with the waves, it can be seen (figure 7) that this component is non-zero only at frequencies higher than those at the equilibrium peak of the wave spectra. Here the pressure lags the waves by about 140°–120°, the corresponding coherences being 0·3–0·5. At frequencies lower than those at the equilibrium peak coherences are higher, 0·5–1·0, and the phase is near 180°. The following results are typical of those found in the other data groups.

(i) There is a range of high frequencies where the pressure measured near the

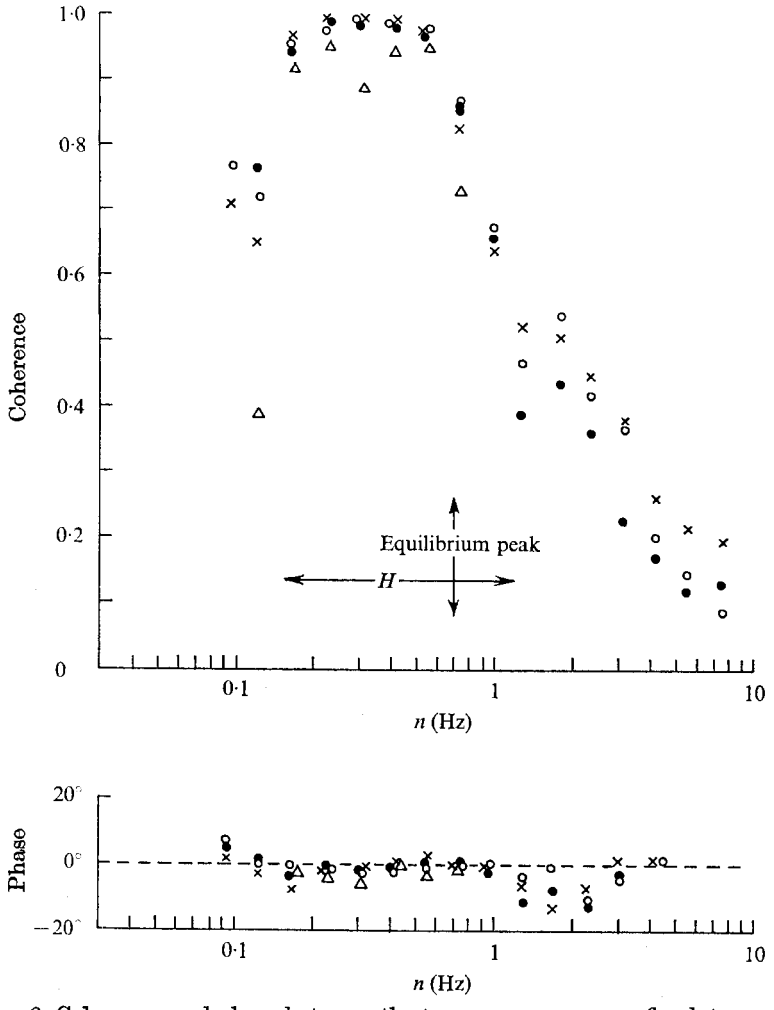


FIGURE 8. Coherence and phase between the two pressure sensors for data group *B*. Phase positive means that the signal at the lower pressure sensor leads that at the upper. ●, run 60/4; ×, run 119/1; ○, run 119/2; △, run 119/3.

wave crests shows significant quadrature with the waves, this may include all waves of frequency higher than the frequency at the equilibrium peak.

(ii) There may be other lower frequency waves (see figure 1, run 119/2) which can be interpreted to be waves generated elsewhere and propagating into the region, where the phase is near 180° and coherences are higher (see figure 7, run 119/2).

In group *B* there was a second pressure sensor (measuring $p_U$) 50 cm above the lower one. The coherence and phase between these two sensors are shown in figure 8. Data not associated with waves, at $n < 0{\cdot}1$ Hz, are not plotted. Phases between $p_L$ and $p_U$ are near zero, $\pm 5°$ throughout the extent of the hump, *H*. Thus the large phase shift between the static pressure and the waves occurs below the lower pressure sensor, with almost no shifting occurring in the next 50 cm vertically above.

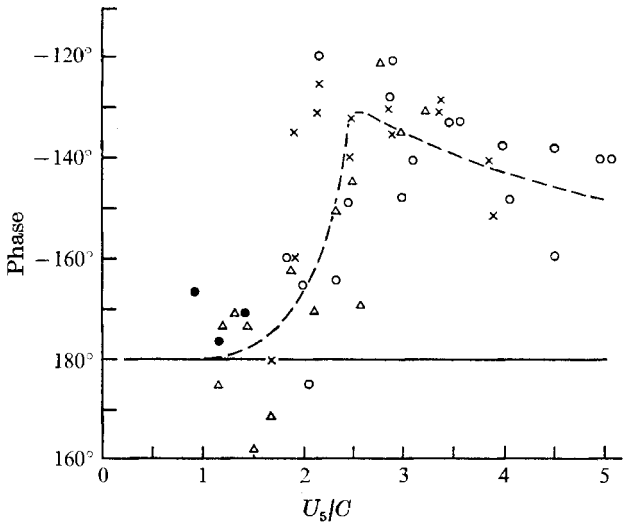


FIGURE 9. Phase shift between pressure and waves at various values of $U_5/C$. Phase positive means the pressure leads the waves. ○, data group $A$; ×, data group $B$; △, data group $C$; ●, data group $D$.

All the $p$–$\eta$ phase information for frequencies within the extent of the equilibrium wave spectrum ($\Phi_\eta(n) \propto n^{-5}$) are plotted in figure 9 against $U_5/C$, which is representative of the relative speed between the mean wind at 5 m and the phase speed of the waves. (The restriction that the data are for the frequencies within the range of the equilibrium wave spectrum is equivalent to the restriction used to develop (5).) In view of the results given in the above paragraph, the $p$–$\eta$ phase relationship is not a strong function of the observation height and data taken at different heights may be compared. As shown by figure 9, the phase between pressure and waves necessary for wave generation occurs for $U_5/C > 2$ and does not show any further shift from 180° for increasing $U_5/C$; in fact, if anything, the opposite appears to be true. For $U_5/C < 2$, phases are near 180°, the phase expected for potential flow. For the data not plotted (because they were outside the range of the equilibrium wave spectrum) most had $0 < U_5/C < 2$ and one case, interpreted to be for waves travelling against the wind, had $U_5/C < 0$. The $p$–$\eta$ phases for the unplotted data were 180° ± 10° with no definite trend.

The fact that the large $p$–$\eta$ phase difference occurs at values of $U_5/C$ greater than about 2 is thought to be due to the height of the critical level relative to the wave amplitude $\eta_a$ for these particular groups of data. The 'critical height' $z_c$ is the height at which $U = C$ (Phillips 1966, p. 92). In the present data, at values of $U_5/C \simeq 2$ the critical height approaches a value equal to the wave amplitude. For example, if a logarithmic wind profile and a roughness length of 0·01 cm are assumed (this value of roughness length is approximately equivalent to a drag coefficient $C_D = 1{\cdot}2 \times 10^{-3}$ at 5 m) it is found that $z_c \simeq \eta_a$ at 0·6 Hz in data group $B$. As is shown in figure 7, the shift from 180° occurs for $n \geqslant 0{\cdot}6$ Hz. Thus the apparent restriction of $U_5/C \gtrsim 2$ for significant wave growth may be due to a requirement of $z_c \lesssim \eta_a$. When the critical height is below the wave amplitude

the air at the level of the wave crests is moving faster than the phase speed of the waves. The data, and therefore this interpretation, apply to a well-developed wave field only and not to initial wave growth.

The phase distribution given by Dobson (1971, figure 8) cannot be compared directly with the present results because his values are for measurements at the wave surface and include the influence of $\rho g \eta_a$, the instrument motion. If $\rho g \eta_a$ is removed from his signal, a first approximation to correct for the motion of his instrument, the phase distribution is comparable with that shown in figure 9; the scatter is larger than for the present data, the shift from 180° appears to increase continuously with increasing $U_5/C$ rather than decrease as does the present data and values at $U_5/C > 2$ are larger than those in the present results by 20°–50°.

In summary, significant wave generation appears to occur in the present data only when $U_5/C \gtrsim 2$. This is equivalent to having the critical height near or below the wave amplitude. Typical phase shifts measured above the wave crests during generation indicate that pressure lags the waves by about 140° and does not change appreciably with height or relative wind speed for the range measured (approximately $2 \leqslant U_5/C < 7$ and $0{\cdot}5 < kz < 3$). Even though the pressure fluctuations associated with the waves are up to one order of magnitude larger than those expected to be present owing to random turbulence, the coherence with the waves is only about 0·3–0·5. When the critical height is well above the measurement level, coherences are higher and phase shifts near 180°, as is expected for a potential-type flow.

Considering figure 4 in the light of this phase information, a better fit to the amplitude data might be that the lines of constant frequency follow roughly the potential-flow solution for $U_5/C \leqslant 1$, say, and then increase to be asymptotic to straight lines among the data for $U_5/C > 2$.

3.1.3. *Energy flux to the waves.* Even though the energy input to the waves cannot be evaluated directly from the present results, an estimate can be made by extrapolation. The fractional increase in wave energy $\zeta$ per radian is

$$\zeta = \frac{1}{\omega E} \frac{\partial E}{\partial t}, \tag{7}$$

where $\omega$ is the frequency in rad $s^{-1}$, $E$ is wave energy and $\partial E/\partial t$ is the flux of energy into the waves. The energy flux into the waves can be calculated if the pressure $p_\eta$ at the wave surface and the velocity of the surface are known:

$$\frac{\partial E}{\partial t} = \overline{p_\eta \frac{\partial \eta_a}{\partial t}},$$

where $\eta_a$ is wave amplitude. With $E = \frac{1}{2}\rho_w g \eta_a^2$, where $\rho_w$ is the density of water, equation (7) can be rewritten in terms of spectral data as

$$\zeta = (1/\rho_w g)\, Q_{p\eta}/\Phi_\eta. \tag{8}$$

$Q_{p\eta}$ (dyn $cm^{-1}$ $Hz^{-1}$) is the quadrature spectral value between the surface pressure and the wave amplitude; $\Phi_\eta$ ($cm^2$ $Hz^{-1}$) is the spectral value of the wave amplitude. $\rho_w g$ has a value of $10^3$ dyn $cm^{-3}$ approximately.

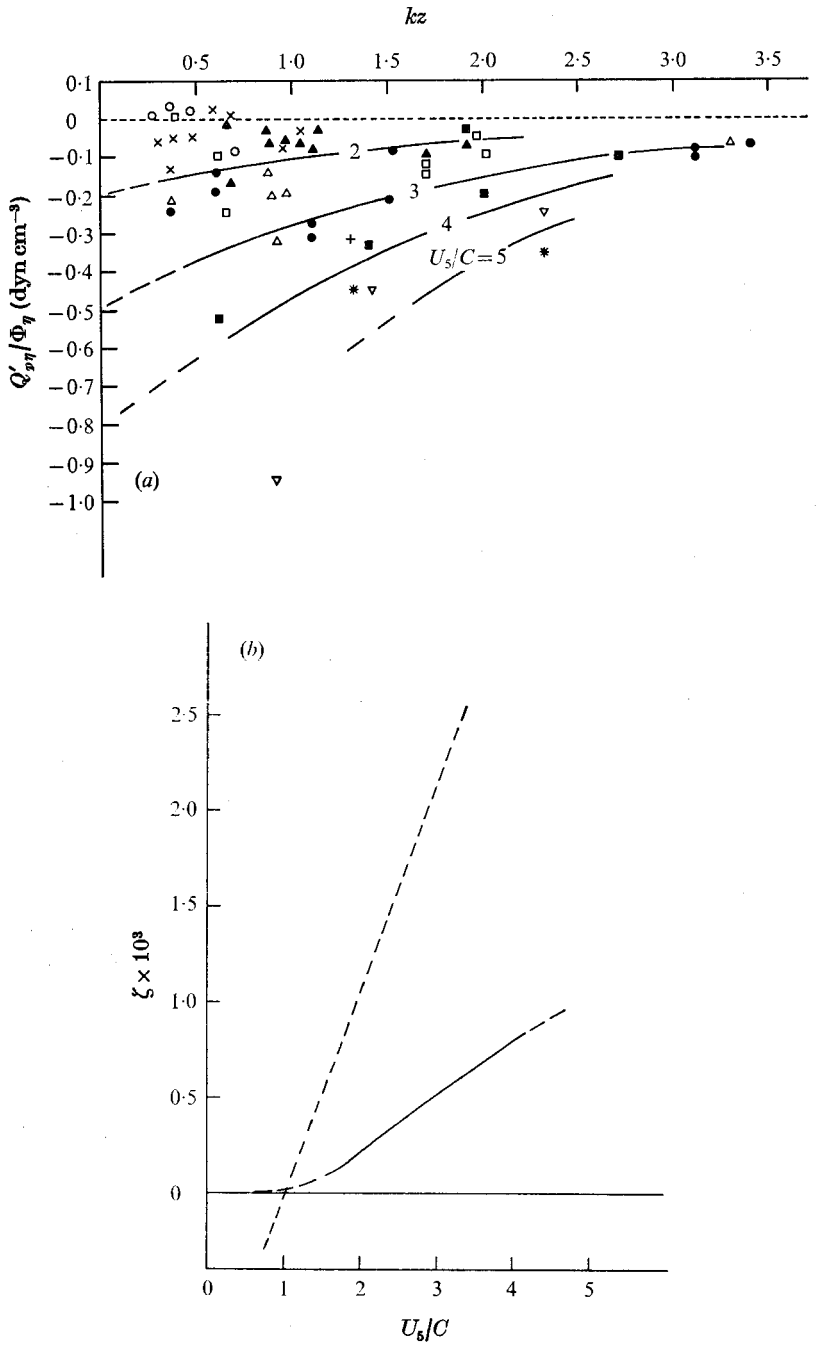


FIGURE 10. (*a*) Values of $Q'_{p\eta}/\Phi_\eta$, representative of the quadrature spectral values between pressure measured above the wave surface and the height of the wave surface, shown as a function of $kz$ and $U_5/C$. ○, $U_5/C$ = 0·5–1·0; ×, 1·0–1·5; ▲, 1·5–2·0; □, 2·0–2·5; ●, 2·5–3·0; △, 3·0–3·5; ■, 3·5–4·0; +, 4·0–4·5; ▽, 4·5–5·0; ✱, 5·0–5·5. (*b*) Fractional increase in wave energy $\zeta$ per radian as a function of $U_5/C$. ——, equation (8); – – – Dobson (1971). The fall-off of $\zeta$ at the higher wave frequencies (larger $U_5/C$) is not shown.

In the present data, the pressure was measured above the wave surface and at a fixed height. To extrapolate the results the assumption is made that the pressure measured at a fixed level differs from that at an oscillating level by a signal which is in phase with the waves and hence does not contribute to the quadrature spectrum. Values of $Q'_{p\eta}/\Phi_\eta$, where $Q'_{p\eta}$ is calculated using the pressure measured at a fixed height above the waves, are plotted in figure 10(*a*) as a function of $kz$ for different values of $U_5/C$. In this plot $k\eta_a$ is approximately constant since the data are taken for the frequency range where the wave spectrum has the equilibrium form with a spectral slope of $-4{\cdot}5$ to $-5$. Lines of constant $U_5/C$ were drawn by hand among the data and extrapolated to $kz = 0$. It is assumed that the values of $Q'_{p\eta}/\Phi_\eta$ at $kz = 0$ are representative of $Q_{p\eta}/\Phi_\eta$ at $z = \eta$. Substitution of values of $Q'_{p\eta}/\Phi_\eta$ at $kz = 0$ into (8) gives $\zeta$ as a function of $U_5/C$; this curve is plotted in figure 10(*b*). The mean curve from Dobson's (1971) measurements has been included for comparison. The present data have a slope of only about half that obtained by Dobson, nevertheless the values are of comparable magnitude and tend to support the large values of $\zeta$ found by Dobson. It is difficult to estimate the errors involved since the validity of the extrapolation down to the wave surface is unknown. Dobson states that errors as large as 50 % may be present in his data at $U_5/C > 4$. No attempt has been made to show the fall-off of the $\zeta$ curve at the higher wave frequencies. Dobson's results, obtained at the same site under similar wind speeds and directions, found a fall-off of the $\zeta$ curve at frequencies above 1·5 Hz. Only a few points at frequencies as high as 1·3 Hz were used in the plot of figure 10(*a*). In all cases the measured pressure became incoherent with the wave height at higher frequencies, partly as a result of the separation of the sensors. A more detailed comparison deserves further experimental study.

### 3.2. *Downstream velocity*

3.2.1. *Spectra.* It is surprising that there is not an obvious 'hump' in the velocity spectra at the frequencies near the peak of the wave spectrum (figure 2) in view of the large increase in energy observed in the pressure spectra. A slight hump is visible in the velocity data of group *D*, the group in which the waves were travelling faster than the wind. For the remaining data the velocity spectra are similar to those observed in the absence of waves; for example, a region where the slope is $-\frac{5}{3}$ exists at the higher frequencies. The velocity ($u$) curve shown in figure 2 is typical.

It is difficult to make an estimation of the expected amplitude of the velocity fluctuations associated with the waves or with the observed pressure since the relationships between them are not known. A rough calculation of the amplitude of the expected velocity fluctuations can be made using data from run 119/2. If it is assumed that the pressure–velocity relationship can be simplified to $\partial u/\partial t + U\,\partial u/\partial x = -(1/\rho)\,\partial p/\partial x$ and that this has a sinusoidal solution, the magnitudes observed for $u = (2\Phi_u(n)\,\Delta n)^{\frac{1}{2}}$ can be compared with those calculated from $u = -p/\rho(U - C)$, where $C$ is the phase speed of the waves. As an example, in run 119/2 (figure 2) at $n = 0{\cdot}55$ Hz ($\Delta n = 0{\cdot}15$ Hz), $p = (2\Pi(n)\Delta n)^{\frac{1}{2}} = 3{\cdot}45$ dyn/cm$^2$ and hence the calculated value of $u = 17$ cm/s. The measured value is also

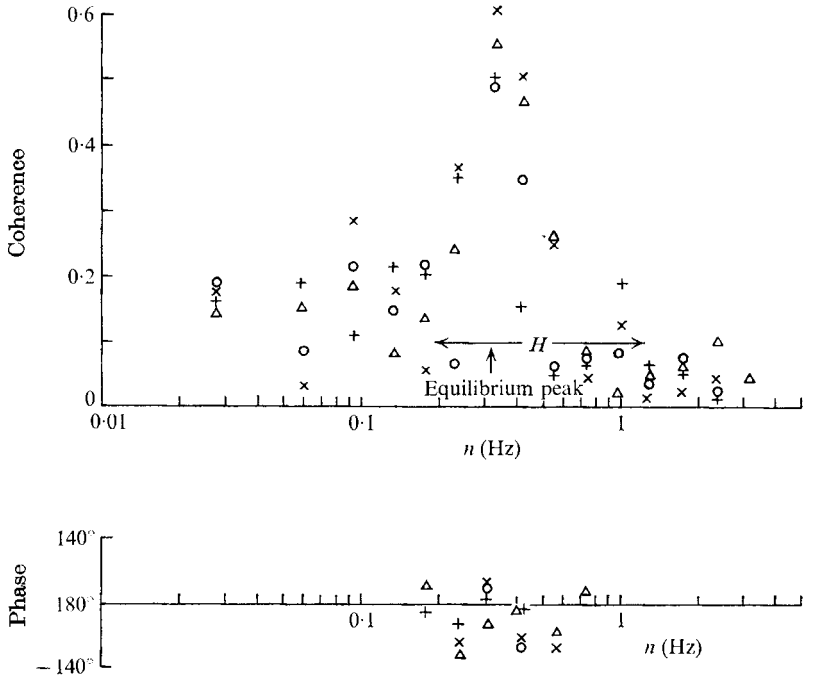


FIGURE 11. Coherence and phase between the $u$ velocity and the waves $\eta$ for data group $C$. Phase positive means that $u$ leads $\eta$. ○, run 60/1; +, run 60/2; ×, run 80/3; △, run 173/3.

17 cm/s. Similarly, at $n = 0{\cdot}73$ Hz ($\Delta n = 0{\cdot}22$ Hz), $p = 2{\cdot}1$ dyn/cm$^2$ and the calculated $u = 16{\cdot}5$ cm/s while the measured $u = 9$ cm/s. However this is only a rough agreement since the relationship between $u$ and $p$ is not known. Nevertheless, the velocities observed may be large enough to correspond with the observed pressures.

3.2.2. *Coherence and phase.* A typical coherence and phase relationship between the measured velocity $u$ and waves $\eta$ is shown in figure 11. These data are from group $C$. At $n \leqslant 4{\cdot}2$ Hz the downstream velocity fluctuations and waves have a phase difference of about 180°, as required for potential-type flow (a velocity fluctuation is positive when in the direction of the mean flow); the coherences are lower than those between the corresponding pressure and waves. At the higher frequencies, $n \geqslant 0{\cdot}55$ Hz, the signals are less coherent (coherence $\leqslant 0{\cdot}1$) and the phases random. The more coherent 180° phase range (in run 164/1, measured $u$–$\eta$ coherences went as high as 0·75), at low frequencies, giving way to a low coherence (coherence $\leqslant 0{\cdot}1$) random phase range, was present in all the other data. The frequency of the transition corresponds to the $p$–$\eta$ phase change at $U_5/C \simeq 2$. The velocity confirms the potential-flow-like behaviour when the critical height is well above the measurement level, but has a random nature when $z_c$ is well below the measurement level.

### 3.3. *Pressure–velocity relationship*

The pressure–velocity cross-correlation for measurements made near the wave surface indicates that the wave field has a strong influence on the turbulence

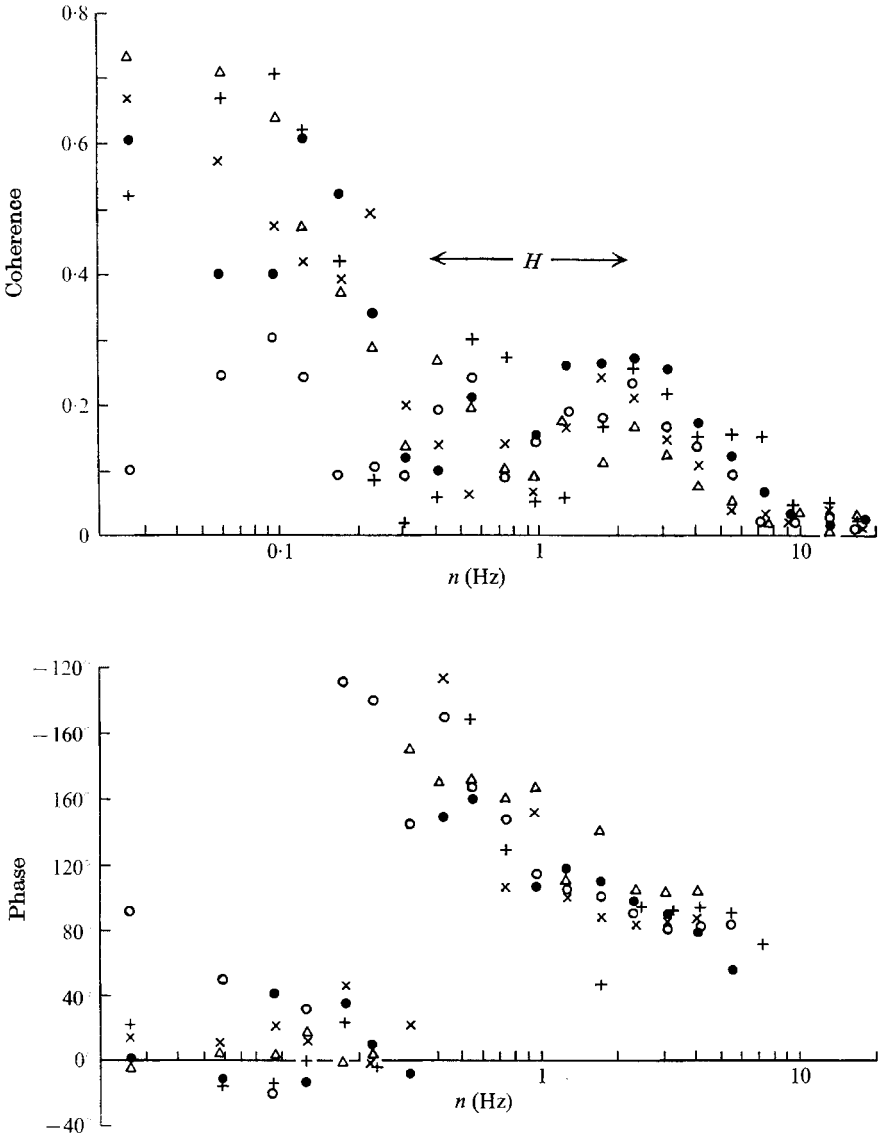


FIGURE 12. Coherence and phase between pressure and $u$ velocity near waves. Phase positive means that pressure leads velocity. ×, run 80/3; ○, run 60/1; ●, run 60/2; △, run 80/2; +, run 60/3.

in the air above. Over a flat boundary it was found by Elliott (1972) that $p$ and $u$ were in phase for those vertical pressure scales that were larger than the height at which the observations were made, shifting to the neighbourhood of 135° at smaller scales. (The vertical scale length $L_p(n)$ of a pressure fluctuation at any given frequency is defined in terms of the coherence between two vertically separated simultaneous measurements of the pressure. The scale length is set equal to the separation at the frequency at which the coherence falls to 0·14. It was found that $L_p \simeq \frac{1}{2}\lambda_p = U/2n$.) Examples of the coherence and phase of $p$

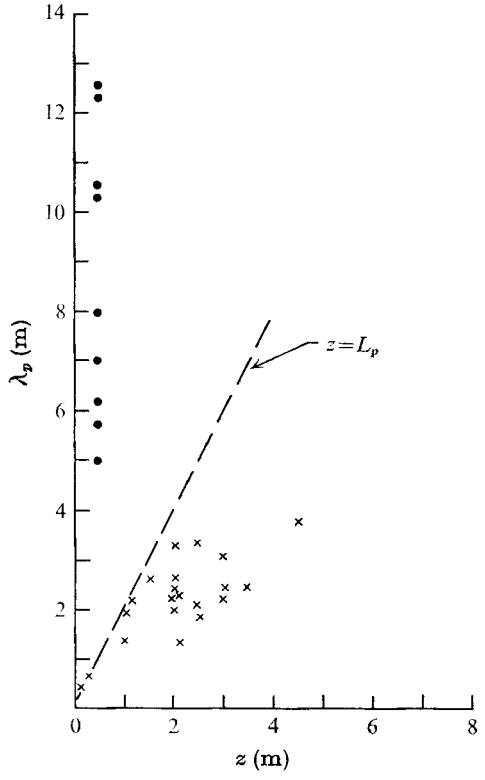


FIGURE 13. Scale length of the pressure fluctuations associated with the $p$–$u$ phase transition. ●, over waves; ×, over a flat surface (Elliott 1972).

and $u$ over waves are shown in figure 12. The general features appear to be the same as those obtained from observations over a flat boundary except for a lower coherence through the region of the pressure hump, labelled $H$. However, the calculated wavelength $\lambda_p = U/n$ at which the phase 'transition' occurs is entirely different, being much larger than over land. Figure 13 shows the wavelength $\lambda_p$ of the pressure at the phase transition compared with those obtained over a flat boundary by Elliott (1972). The scales at the transition are several times larger than those expected over a flat boundary at a similar height. In every case it was found that this phase transition over waves occurs at the frequency of the peak of the pressure hump when the pressure spectra are plotted as $n\Pi(n)$. In most cases this also corresponds to the peak of the $n\Phi_\eta(n)$ wave spectrum. The wavelength of the waves appears to introduce, through the pressure field, a new length scale with which the turbulence interacts.

As with the observations taken over a flat boundary by Elliott (1972), there was a large energy loss from the $u$ velocity component at frequencies above the phase transition. The ratio of the energy flux from the $u$ component caused by pressure forces to the total energy dissipation at the same level can be written as

$$-\frac{\overline{u\,\partial p}}{\partial x}(n)\Big/\rho\frac{u_*^3}{\kappa z},$$

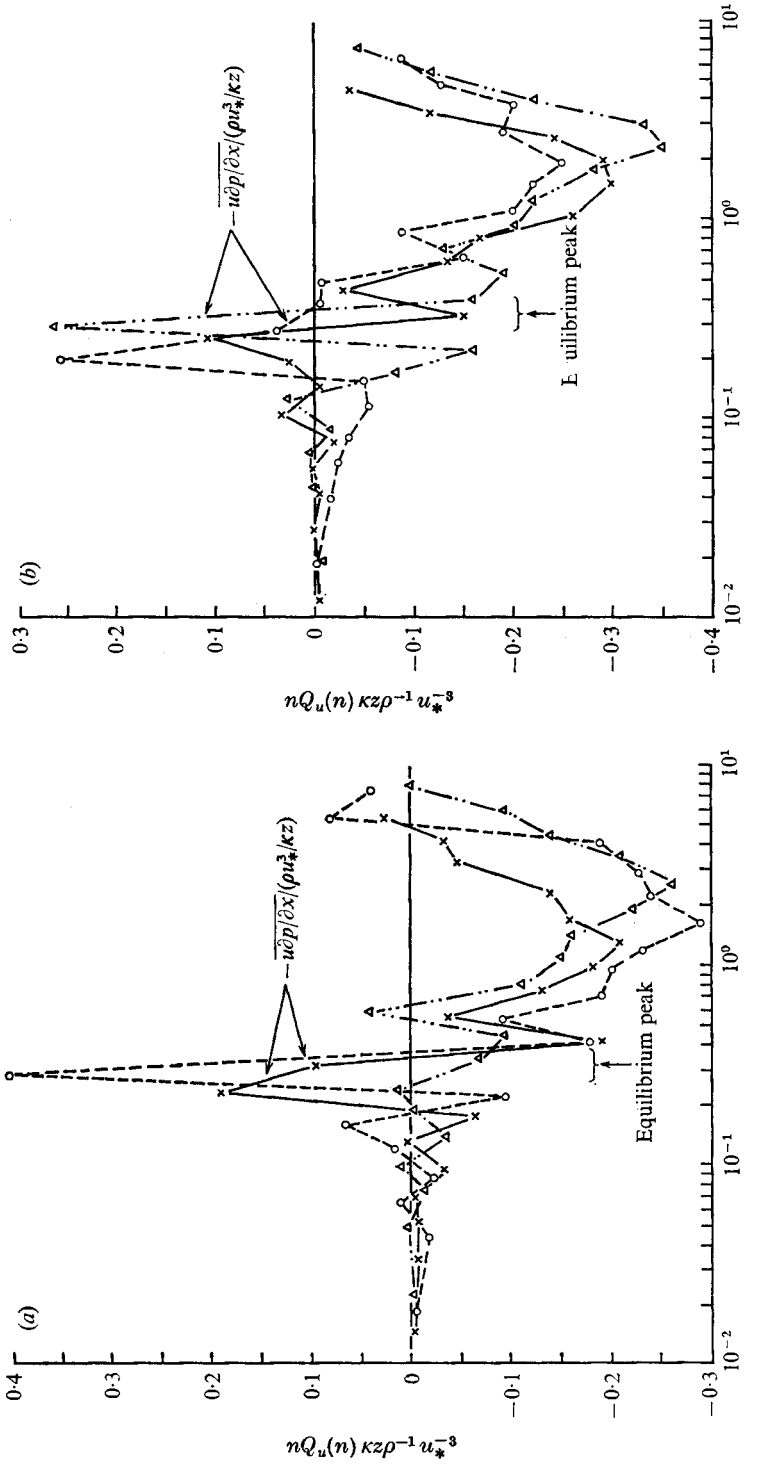


FIGURE 14. Non-dimensional energy flux from the $u$ velocity component, measured near waves. (*a*) ×, run 80/3, integral = −0·22; ○, run 60/1, integral = −0·34; △, run 60/2, integral = −0·37. (*b*) ×, run 119/2, integral = −0·38; ○, run 60/4, integral = −0·34; △, run 119/1, integral = −0·50.

where $\rho u_*^2$ is the surface stress and $\kappa \simeq 0{\cdot}4$ is von Kármán's constant. This energy flux was calculated for the observations over waves using the quadrature spectrum between $p$ and $u$ and applying Taylor's hypothesis. The results are plotted against $kz$ in figures 14($a$) and ($b$). The distribution of energy flux is similar to that found over a flat boundary, with most of the flux occurring at scales immediately above the $p$–$u$ phase difference transition (see figure 12). For those values of $kz$ near the peak of the wave spectrum (see figure 14) the sign of the flux is often positive and the magnitude is highly variable. The integrals under the curves show an energy loss from the $u$ component to the other velocity components similar to that found from data collected over a flat boundary. The integrations for the range $10^{-2} < kz < 10^{1}$ were typically $-0{\cdot}3$ to $-0{\cdot}4$ (see caption to figure 14). Although these values are similar in magnitude to those over a flat boundary, the energy flux begins at a non-dimensional height $kz$ which is lower by an order of magnitude; this change is interpreted to be a result of the turbulence interacting with the waves.

This work was done under R. W. Stewart as part of the Air–Sea Interaction programme at the Institute of Oceanography, University of British Columbia and was partially supported by the U.S. Office of Naval Research under Contract N00014-16-C-0047, Project NR 083-207. Most of the data were analysed using software developed by J. F. Garrett and J. R. Wilson, whom the author thanks.

## REFERENCES

Blackman, R. B. & Tukey, J. W. 1959 *The Measurement of Power Spectra.* Dover.

Dobson, F. W. 1971 *J. Fluid Mech.* **48**, 91.

Elliott, J. A. 1970 Ph.D. dissertation, Institute of Oceanography, University of British Columbia.

Elliott, J. A. 1972 *J. Fluid Mech.* **53**, 351.

Garrett, J. F. 1969 *J. Mar. Res.* **27**, 273.

Hume, D. 1969 *Instruction Manual, Capacitive Wave Probe.* Vancouver: Institute of Oceanography, University of British Columbia.

Lamb, H. 1932 *Hydrodynamics.* Cambridge University Press.

Phillips, O. M. 1966 *The Dynamics of the Upper Ocean.* Cambridge University Press.

Pond, S., Smith, S. D., Hamblin, P. F. & Burling, R. W. 1966 *J. Atmos. Sci.* **23**, 376.

Shemdin, O. H. & Hsu, E. Y. 1967 *J. Fluid Mech.* **30**, 402.